Iranian Journal of Materials Forming 10 (3) (2023) 4-14

Online ISSN: 2383-0042

Iranian Journal of Materials Forming

Journal Homepage: http://ijmf.shirazu.ac.ir

Research Article

Exploring the Impact of Friction Stir Welding Parameters on Mechanical Performance and Microstructure of AZ91C Magnesium Alloy Joints Using Taguchi Method

S. Rouhi[1], A. Doniavi[1*] and M. Shahbaz[2*]

[1] Department of Mechanical Engineering, Faculty of Engineering, Urmia University, Urmia, Iran
[2] Department of Materials Science and Engineering, Faculty of Engineering, Urmia University, Urmia, Iran

ARTICLE INFO

Article history:

Received 21 May 2023
Reviewed 17 June 2023
Revised 31 July 2023
Accepted 19 August 2023

Keywords:

Friction stir welding
Magnesium alloy joints
Experimental design
L9 orthogonal array
Characterization

Please cite this article as:

S. Rouhi, A. Doniavi, M. Shahbaz, Exploring the Impact of Friction Stir Welding Parameters on Mechanical Performance and Microstructure of AZ91C Magnesium Alloy Joints Using Taguchi Method, *Iranian Journal of Materials Forming*, 10 (3) (2023) 4-14

ABSTRACT

In this study, we investigated the influence of process parameters on the mechanical properties of AZ91C magnesium alloy joints produced by friction stir welding (FSW). A Taguchi L9 orthogonal array was employed to design the experimental matrix, and the input variables were analyzed. Tensile strength and hardness values were measured for different input parameters, and their interactions were assessed through interaction plots for ultimate tensile strength (UTS) and Vickers hardness (HV). The signal-to-noise (S/N) ratios were calculated, and S/N ratio plots were generated to further understand the effects of the input parameters on the mechanical properties. Microstructural evaluations were carried out on the base metal and stir zone (SZ) of the specimens produced under various process conditions. Additionally, the appearances of the FSW samples with the minimum and maximum tensile strengths were compared.

The results revealed complex relationships between the process parameters and mechanical properties, with both main effects and interactions playing significant roles in determining the performance of the FSW joints. Notably, an optimal combination of process parameters (tool rotation speed of 1250 rpm, welding speed of 40 mm/min, and plunge depth of 0.3 mm) resulted in the highest ultimate tensile strength (UTS) and hardness (HV) values. Microstructural analysis showed that FSW significantly refined the grain size, contributing to the improvement of mechanical properties.

1. Introduction

In recent years, magnesium alloys have gained significant attention due to their excellent strength-to-weight ratio and potential applications in various industries, particularly the automotive sector. Among magnesium alloys, the AZ91C magnesium alloy has been widely used for automotive applications.

However, its use is limited by low mechanical properties at moderate temperatures. To overcome this limitation, researchers have employed various techniques, such as alloy development, addition of reinforcements, and local materials engineering [1-5].

Friction stir welding (FSW) is a promising method for joining AZ91C magnesium alloy components and has been recognized as an energy-efficient,

* Corresponding authors
E-mail addresses: mehredads1@gmail.com (M. Shahbaz),
E-mail addresses: a.doniavi@urmia.ac.ir (A.Doniavi)
https://doi.org/10.22099/IJMF.2023.47437.1258

environmentally friendly, and versatile joining technique.

The FSW process involves several parameters, including tool rotation speed, welding speed, and plunge depth, which significantly influences the quality and mechanical properties of the welded joints [6-8]. Previous research has investigated the effects of welding parameters on microstructure, mechanical properties, and residual stress profiles of FSW joints [9-13]. Some researchers have also studied the joining of dissimilar magnesium alloys and aluminum using FSW [14, 15]. In the existing studies of Friction Stir Welding [9, 10, 12, and 13], it's pointed out that the resultant microstructure can be categorized into three unique areas: the heat-affected zone (HAZ), thermo-mechanically affected zone (TMAZ), and stirred zone (SZ). The SZ is characterized by a uniformly distributed recrystallized grain structure with small, equiaxed grains. This is obtained through the process of dynamic recrystallization (DRX) that occurs within the deformed region [16].

The execution of friction stir welding involves a number of key operational inputs [7], listed here in the decreasing order of their impact: 1) speed of the tool rotation, 2) welding speed, 3) design of the tool, 4) tilt angle, 5) axial load, 6) plunge depth, and 7) backing plate. The friction stir welding process mainly revolves around two significant parameters: the rotation speed of the tool and the speed of welding. These two factors have a substantial effect on the quality and mechanical attributes of the joints produced by friction stir welding.

In this study, we aim to optimize the FSW process parameters for AZ91C magnesium alloy and investigate their impacts on ultimate tensile strength (UTS) and hardness (HV) using the design of experiments approach. To perform analyses and the optimization, a series of experiments were designed using the Taguchi L9 orthogonal array [17]. Tool rotation speed, welding speed, and plunge depth were considered as the input parameters. The main effects and interactions of the process parameters were analyzed, and the signal-to-noise (S/N) ratio was calculated to evaluate the performance characteristics. An analysis of variance (ANOVA) was carried out to evaluate the impact of each process parameter on the mechanical attributes [17].

In addition to the primary focus of this study, it is essential to acknowledge and build upon relevant earlier works in the field. The study about thermo-mechanically affected zone in friction stir welding sheds light on the intricate thermal and mechanical changes that occur in the welding process, impacting the microstructure and mechanical properties of the joints [18]. Moreover, studying about friction stir lap welding of aluminum to brass contributes to the understanding of joining dissimilar materials through FSW, providing valuable insights into material mixing and intermetallic formation [19]. By integrating and expanding upon these findings, our research endeavors to address the challenges faced in optimizing the FSW process parameters for AZ91C magnesium alloy joints and enhancing their mechanical properties for potential applications in the automotive and aerospace industries.

2. Experimental Procedure

For this study, a commercially accessible cast ingot of AZ91C magnesium alloy was selected. The chemical composition of the alloy in its as-cast state is detailed in Table 1, while Table 2 provides an overview of its mechanical characteristics. To prepare the specimens for friction stir welding (FSW), the ingot was machined into rectangular plates with a thickness of 8 mm. The friction stir welding (FSW) process was conducted using a special designed fixture to secure the workpieces during welding, as illustrated in Figure 1(a). The FSW tool was constructed from the AISI H13 hot-working tool steel and featured a square pin shape. The tool had an 18 mm shoulder diameter and a square pin with a cross-section of 4.25 × 4.25 mm^2 and a length of 5 mm, as shown in Figure 1(b). The FSW tool was set to operate in a clockwise motion with a 3° inclination.

Table 1. Chemical composition of the AZ91C magnesium alloy in its as-cast state

Element	Mg	Al	Zn	Mn	Si	Fe	Cu	Ni
Weight (%)	Bal.	8.9	0.84	0.33	0.07	0.01	0.004	0.87

Table 2. Mechanical properties of the AZ91C magnesium alloy in its as-cast state

Base metal	Tensile strength (N/mm^2)	Elongation (%)	Hardness (HV)	Grain size (µm)
As-cast AZ91C	140	6.74	81	90

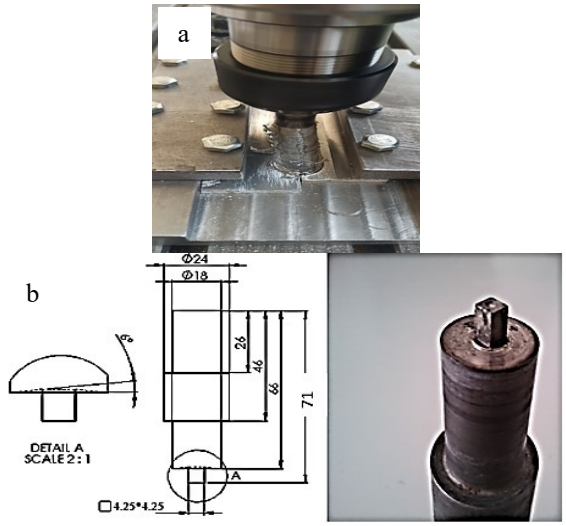

Fig. 1. (a) Shows the experimental set-up of FSW machine (b) dimensions of AISI H13 hot working tool steel used to in preparing FSW joints in *mm* and used fixture in FSW joint.

Standard metallographic techniques were employed to prepare the transverse sections of the specimens for microstructural analysis. The prepared specimens were then etched using a solution composed of 60 vol. % ethylene glycol, 19 vol. % acetic acid, 1 vol. % HNO3, and 20 vol. % H2O for a duration of 1 minute. The microstructure of the base metal and stir zone (SZ) of the specimens produced under various process conditions was examined using optical microscopy. Tensile examinations were carried out at room temperature using a universal tensile testing apparatus at a rate of 1 mm/min. The specimens' dimensions for this test complied with the ASTM EM08 standard, as illustrated in Figure 2. The ultimate tensile strength (UTS) was determined from the tensile test results.

Microhardness evaluations were conducted at locations 1 mm beneath the top surface of the specimens and were separated by 2.5 mm from one another. Vickers microhardness tester was used under a 100 g load for a duration of 10 seconds to obtain hardness values (HV).

To systematically investigate the effects of the process parameters on the mechanical properties, a series of experiments were designed using the Taguchi L9 orthogonal array [17]. The main process parameters considered were the tool rotation speed, welding speed, and plunge depth. Table 3 shows the levels and parameters of the process, and Table 4 presents the L9 orthogonal array used to define the experimental setup. The friction stir welding was carried out for each of the nine combinations of process parameters based on the predefined input parameters, utilizing a modified milling machine adapted for friction stir welding. The welding direction was set perpendicular to the rolling direction, and single-pass welding methods were applied to create the joints. During the process, the tool's rotation enabled the stirring and blending of materials around the spinning pin, transporting material from the pin's front to its back, thereby finalizing the welding process. The welding speed, tool rotation speed, and plunge depth were strictly controlled during the welding process to ensure consistent and accurate data collection.

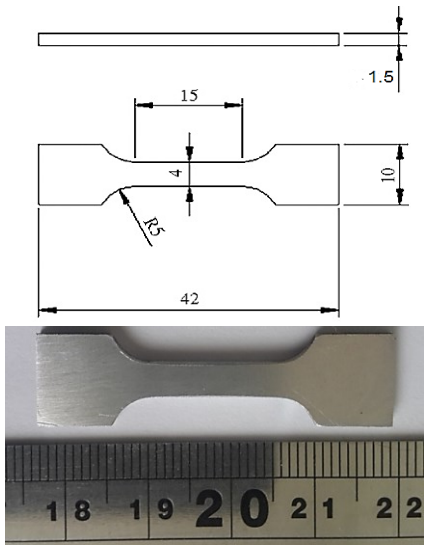

Fig. 2. Schematic representation of the specimen used in the tensile test.

Table 3. Levels and parameters of the process

Parameter	Range	Level 1	Level 2	Level 3
Tool rotation speed (rpm)	800-1600	800	1250	1600
Welding speed (mm/min)	20-60	20	40	60
Plunge depth (mm)	0.2-0.4	0.2	0.3	0.4

Table 4. L9 orthogonal array or input variables

Experiment no.	Tool Rotation speed (rpm)	Welding speed (mm/min)	Plunge depth (mm)
1	800	20	0.2
2	1250	40	0.2
3	1600	60	0.2
4	800	60	0.3
5	1250	40	0.3
6	1600	20	0.3
7	800	60	0.4
8	1250	20	0.4
9	1600	40	0.4

After FSW, microstructural evaluations were performed to examine the grained structure and other microstructural features of the base metal and SZ for each combination of process parameters. Additionally, the appearances of the FSW samples, with the minimum and maximum tensile strengths, were compared to visually observe the surface quality and weld line characteristics.

3. Results and Discussion

3.1. Statistical results from Taguchi method

The results of the ultimate tensile strength (UTS) and hardness values for the designed experiments are presented in Table 5. A wide range of UTS values were observed, with a minimum value of 156.8 MPa in experiment 1 and a maximum value of 245.6 MPa in experiment 5. The hardness values also exhibited noticeable variations, ranging from a low of 90 HV in experiment 1 to a high of 113 HV in experiment 6. The findings indicate that the diverse combinations of process parameters utilized in the experiments substantially influenced the mechanical attributes of the joints created through friction stir welding. Notably, experiment 5 displayed the highest UTS and one of the highest hardness values, indicating a possible optimal combination of process parameters for achieving improved mechanical properties. Conversely, experiment 1 resulted in the lowest UTS and hardness values, suggesting that the specific set of parameters used in this experiment may not be suitable for obtaining desirable mechanical characteristics. The data highlights the importance of selecting appropriate welding process parameters to ensure the production of high-quality joints with enhanced mechanical properties. Further analysis and optimization of the process parameters could provide valuable insights into the underlying relationships between the input variables and the mechanical performance of the resulting welded joints.

Table 5. Tensile strength and hardness values corresponding to varying input parameters

	Tool rotation speed (rpm)	Welding speed (mm/min)	Plunge depth (mm)	Tensile strength (MPa)	Hardness (HV)
1	1250	40	0.2	234.9	93
2	1600	60	0.2	163.3	102
3	800	60	0.3	185.6	105
4	1250	40	0.3	245.6	110
5	1600	20	0.3	210.3	113
6	800	60	0.4	177.6	99
7	1250	20	0.4	239.6	107
8	1600	40	0.4	191.3	109

The main effects represent the average change in the response variable as the factor changes from one level to another. A positive main effect indicates that an increase in the factor level leads to an increase in the response. Conversely, a negative main effect denotes that an increase in the factor level results in a decrease in the response.

Results of running a Matlab code, presented as step-by-step as a text in Figure 3, written for the calculation of the main effects of the parameters showed that

- For UTS, an increase in tool rotation speed and plunge depth results in increasing UTS values, with main effects of 7.4833 and 8.9167, respectively. On the other hand, an increase in

welding speed leads to a decrease in UTS, with a main effect of -13.3667.

- For HV, an increase in tool rotation speed and plunge depth results in increased HV values, with the main effects of 5.0000 for both factors. Conversely, an increase in welding speed leads to a slight decrease in HV, with a main effect of -0.6667.

1. Start

2. Initiate Input Data which includes experiments matrix and UTS, HV vectors

3. Call the MainEffects function with experiments and UTS as inputs

3.1 Enter the function MainEffects

3.1.1 Set n_levels as 3

3.1.2 Set factors as number of columns in experiments matrix

3.1.3 Initialize mainEffects as a zero matrix with size n_levels x factors

3.1.4 Start loop for 'factor' from 1 to 'factors'

3.1.4.1 Start loop for 'level' from 1 to 'n_levels'

3.1.4.1.1 Create a mask vector to find the corresponding rows with the current factor and level in experiments matrix

3.1.4.1.2 Find the mean of elements in response vector where mask vector is true, and assign it to the corresponding element in mainEffects matrix

3.1.4.2 End 'level' loop 3.1.5 End 'factor' loop

3.2 Return from the function MainEffects with mainEffects matrix as output

4. Store the returned values from MainEffects function into main_effects_UTS

5. Call the MainEffects function with experiments and HV as inputs 5.1 Repeat steps from 3.1 to 3.2

6. Store the returned values from MainEffects function into main_effects_HV

7. End

Fig. 3. Structure of the Matlab code step-by-step written for calculation of main effect of parameters.

These results suggest that the welding speed has the most significant impact on the UTS, while tool rotation speed and plunge depth have a more substantial effect on HV. Further analysis or experimentation may be conducted to optimize the process parameters and understand any interactive effects between the factors.

To investigate potential interactions between the process parameters, 2D line plots (Figures 4 and 5) were generated for each pair of parameters. The plots provide a visual representation of the interaction effects, enabling the identification of trends and patterns that may warrant further investigation. From the interaction plots (Figure 4), it was observed that the combinations of tool rotation speed and welding speed, as well as welding speed and plunge depth, exhibited noticeable interactions for UTS than the combination of tool rotation speed and plunge depth. However, it is evident that the combination of tool rotation speed and welding speed exhibits a significant interaction effect on the UTS. As it was shown in Figure 4, the combination for each pair of three parameters show the interaction for HV. Similarly for the case of UTS, the combination of tool rotation speed and welding speed exhibits a significant interaction effect on the HV.

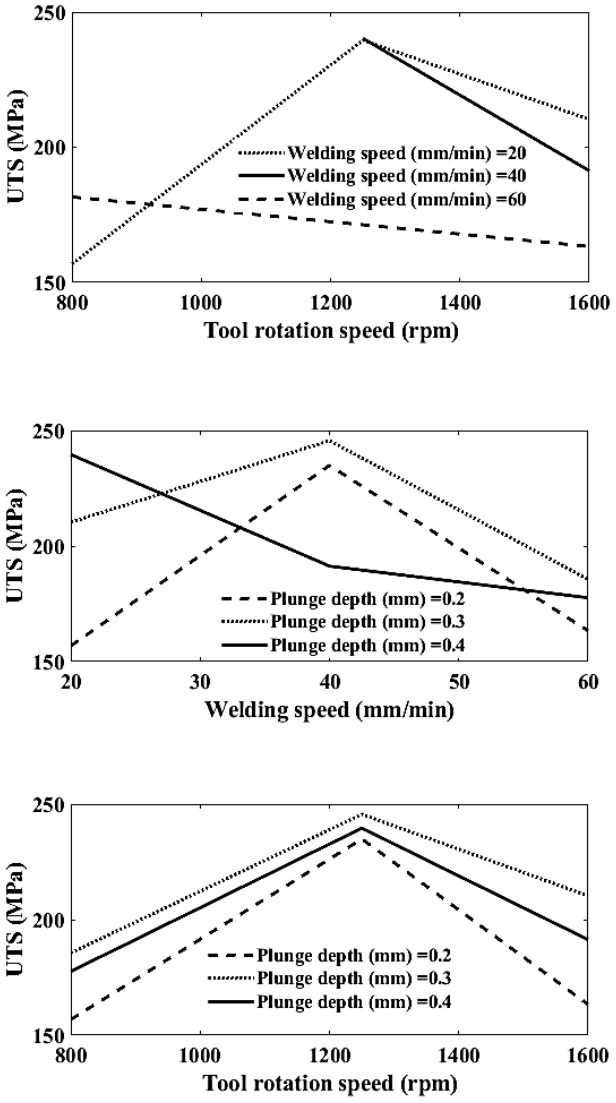

Fig. 4. Interaction plot for UTS.

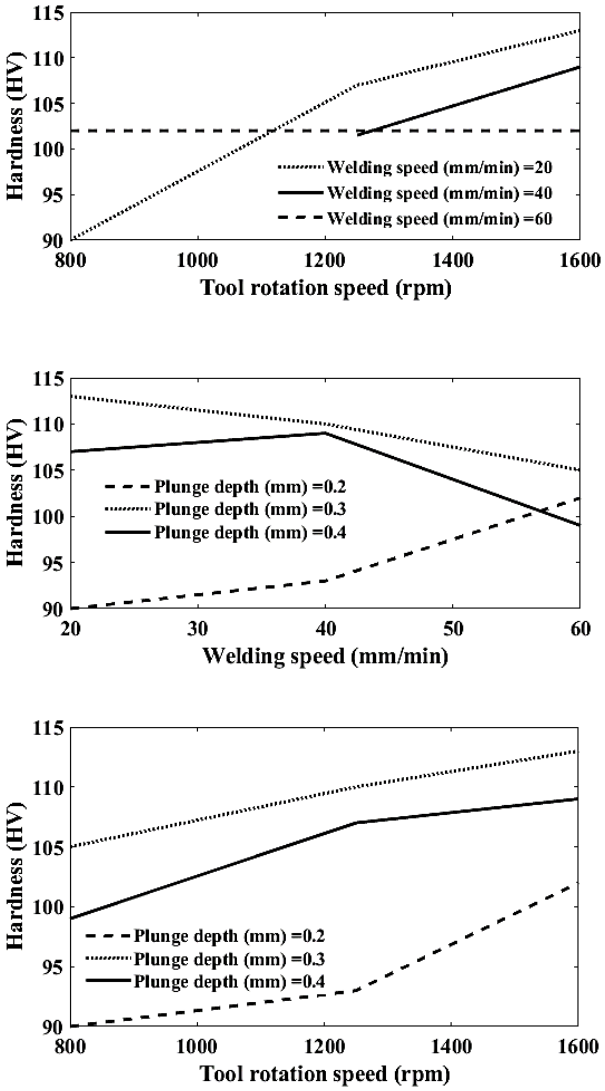

Fig. 5. Interaction plot for HV.

To evaluate the impact of factors on the response, it is possible to calculate the means and signal-to-noise ratios (S/N) for each control factor. In this research, the S/N ratio was selected based on the 'larger-the-better' criterion to maximize the response. The S/N ratio, a logarithmic function of the desired output, functions as the objective function for optimization. It aids in data analysis and prediction of optimal outcomes. The S/N ratio is calculated using the 'larger-the-better' criterion as given by Eq. (1) [17], where Y represents the observed data and n stands for the number of observations. The measured tensile strength and hardness were converted into S/N ratios. The experimental findings and computed S/N ratio values are compiled in Table 6.

$$S/N = -10*\log\left(\Sigma\left(1/Y^2\right)/n\right) \quad (1)$$

Table 6. Results of the experiments and their associated signal-to-noise ratios

Input Parameter			Response		S/N Ratio	
Tool rotation speed (rpm)	Welding speed (mm/min)	Plunge depth (mm)	Tensile strength (MPa)	Hardness (HV)	UTS	HV
800	20	0.2	156.8	90	43.91	39.08
1250	40	0.2	234.9	93	47.42	39.37
1600	60	0.2	163.3	102	44.26	40.17
800	60	0.3	185.6	105	47.6	40.42
1250	40	0.3	245.6	110	47.2	40.83
1600	20	0.3	210.3	113	46.46	41.06
800	60	0.4	177.6	99	44.99	39.91
1250	20	0.4	239.6	107	47.32	40.59
1600	40	0.4	191.3	109	45.63	40.75

From the S/N ratio results for UTS (Table 6 and Figure 6), it can be observed that the highest S/N ratio of 47.60 was achieved at a tool rotation speed of 800 rpm, a welding speed of 60 mm/min, and a plunge depth of 0.3 mm. This indicates that this combination of parameters is the most favorable for obtaining the highest UTS, as higher S/N ratios correspond to better performance under the larger-the-better criterion.

Similarly, from the S/N ratio results for HV (Table 6 and Figure 7), the highest S/N ratio of 41.06 was obtained at a tool rotation speed of 1600 rpm, a welding speed of 20 mm/min, and a plunge depth of 0.3 mm. This suggests that this combination of parameters is the most favorable for achieving the highest HV.

The Taguchi method focuses on optimizing the S/N ratio and finding the best parameter settings by analyzing the main effects and interactions. It assumes that the effect of each factor is independent of the other factors. However, this assumption might not hold true in all cases, as there could be significant interactions between factors that affect the response variables. In such situations, relying solely on the main effects and S/N ratios might not provide a complete understanding of the underlying relationships.

On the other hand, analysis of variance (ANOVA) is a more general statistical method that accounts for the interactions between factors and their effects on the response variables. The ANOVA test checks the null hypothesis, which asserts that there is no substantial difference between the means of the various levels associated with each factor. If the p-value is greater than the significance level (usually 0.05), we fail to reject the

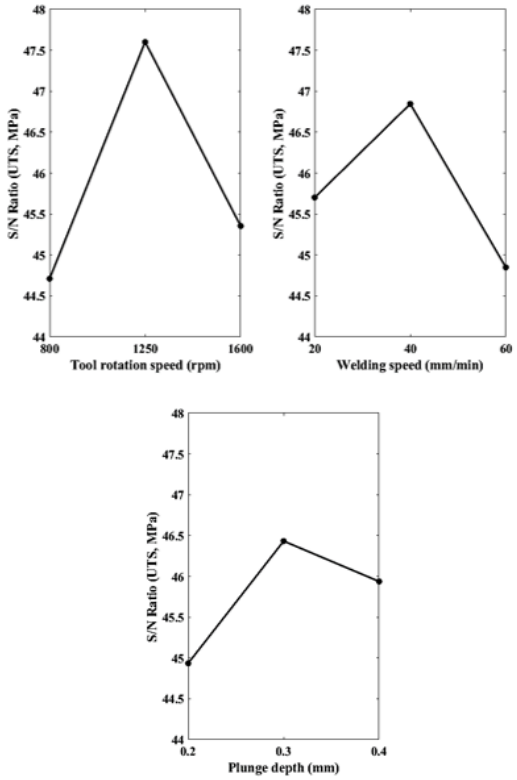

Fig. 6. S/N ratio plot UTS for different input parameters.

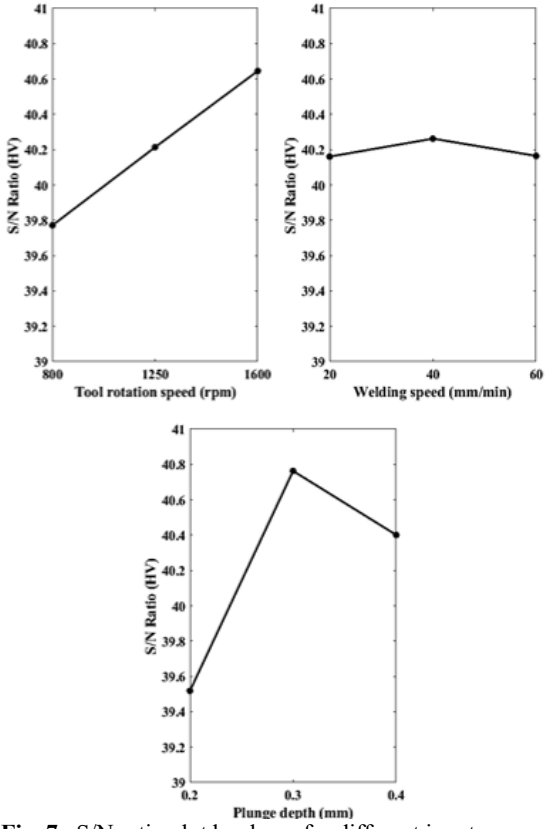

Fig. 7. S/N ratio plot hardness for different input parameters.

null hypothesis and conclude that the factor does not have a statistically significant effect on the response variable. In this study, the ANOVA results suggest that none of the factors have a statistically significant effect on the response variables.

3.2. Microstructure observation and hardness test

The microstructural examinations of the magnesium friction stir welds have provided valuable insights into the grain structure within the stir zone (SZ). This region typically exhibits an equiaxed grain structure, often identified as recrystallized. Figure 8 offers a detailed depiction of the microstructure of both the base metal and the SZ in the friction stir welded (FSWed) specimens.

The base metal's microstructure, as illustrated in Figure 8(a), comprises of coarse grains with sizes varying between 200 to 320 µm. In contrast, the FSWed samples display much smaller, recrystallized equiaxed grains, typically around 16-20 µm in size. A noteworthy observation is the difference in grain structure between the two FSWed samples. The sample created with a rotation speed of 1250 rpm and a welding speed of 40 mm/min exhibits a finer grain structure compared to the one created with a rotation speed of 800 rpm and a welding speed of 40 mm/min. This observation underscores the pivotal role of process parameters in shaping the microstructure and, consequently, the properties of the weld.

The FSW process induces a disturbance that creates conditions conducive to dynamic recrystallization, leading to a reduction in grain size. Dynamic recrystallization can be categorized into continuous and discontinuous types. During the process, the material undergoes severe plastic deformation, resulting in the formation of numerous grain boundaries with minor angle misalignments. The transformation of low-angle grain boundaries to high-angle grain boundaries is referred to as continuous dynamic recrystallization.

The nucleation of new grains occurs in preferred areas such as existing grain boundaries and regions

with high stored energy, leading to a distinct type of recrystallization known as discontinuous dynamic recrystallization. Given sufficient time and heat, new small grains begin to grow, driven by the reduction of grain boundary surface area and the achievement of the lowest energy state.

Therefore, an increase in the rotational speed escalates the amount of heat produced and accelerates the grain growth rate. At a rotation speed of 800 rpm, the grain size is approximately 16 µm, while at a rotation speed of 1250 rpm, it is around 20 µm. Despite the finer grains at 800 rpm compared to 1250 rpm, this can be attributed to the lower disturbance at 800 rpm, which prevents a significant rise in temperature. Moreover, at 800 rpm, the temperature required for the material to become semi-solid is lower. Consequently, the material lacks the ability to become semi-solid, and the welding tool acts more like a machining tool, inhibiting the creation of a joint.

This detailed analysis of the microstructural changes induced by the FSW process and the influence of process parameters provides a deeper understanding of the mechanisms underlying the observed variations in grain structure and its mechanical properties. Further research could explore the optimization of process parameters to achieve desired microstructures and mechanical properties, contributing to the development of more efficient and effective FSW processes.

Figure 9 presents a comparison between the welded samples that achieved the highest (1250 rpm, 40 mm/min, 0.3 mm) and lowest ultimate tensile strength (800 rpm, 20 mm/min, and 0.2 mm). The sample produced at the highest rotation speed exhibits superior surface quality, characterized by a smooth and uniform appearance. In contrast, the sample produced at the lowest rotational speed displays a less desirable weld line, marked by voids and surface irregularities.

This stark contrast between the two samples underscores the profound influence of process parameters on the macrostructure of the weld. The specimen with the higher tensile strength demonstrates a more homogeneous and consistent structure, as opposed to the one with the lower tensile strength (as shown in Figure 8). These images serve as a powerful visual representation of the correlation between process parameters and their impact on the weld's morphology. More specifically, they highlight how variations in process parameters can lead to significant changes in the weld's surface quality and structural consistency, which in turn, directly affect its tensile strength. It's worth noting that the surface quality and structural consistency of the weld are critical factors that determine its mechanical performance. The

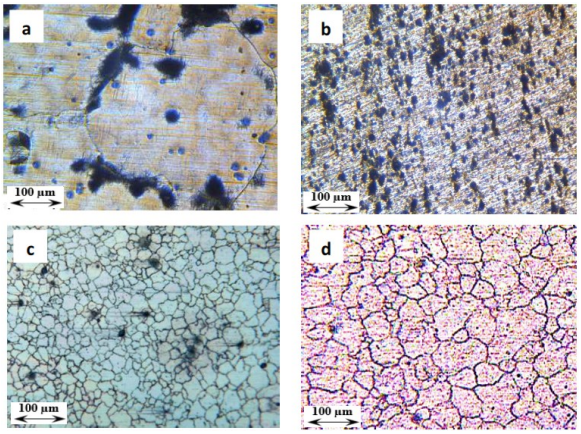

Fig. 8. Microstructure of (a) base metal, and the SZ in the specimens produced with (b) rotational speed 800 rpm, (c) rotational speed 1250 rpm and (d) rotational and traverse speed 1600 rpm and 40 mm/min, respectively.

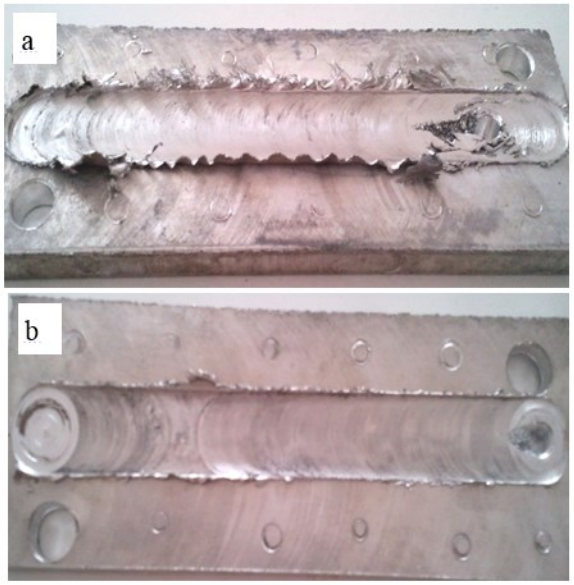

Fig. 9. Visual representation of friction stir welded samples with the (a) lowest and (b) highest tensile strength.

presence of voids and surface irregularities, as seen in the sample produced at the lower rotational speed, can act as stress concentrators, potentially leading to premature failure under tensile loading.

On the other hand, the smooth and uniform surface of the sample produced at the higher rotational speed suggests a more efficient material flow during the welding process, resulting in a weld with superior mechanical properties. This observation reinforces the importance of optimizing process parameters in friction needed in stir welding to achieve high-quality welds with enhanced mechanical performance.

Figure 10 provides a visual representation of the hardness values distribution for the microstructure depicted in Figure 8. The mechanical properties of the samples are influenced by three fundamental factors, as discussed below:

1. The Friction Stir Welding (FSW) process that plays a crucial role in eliminating voids in the casting alloy. Voids are known to contribute to reduced mechanical properties, and their elimination through FSW enhances the overall mechanical performance of the samples [11].
2. The precipitation of Mg17Al12 at the grain boundaries is another significant factor. Grain boundaries are favorable locations for crack nucleation [11]. L. ížek et al. [20] discovered that in heat-treated samples, these precipitations dissolve at high temperatures. Simultaneously, as the samples cool, very fine Mg17Al12 beta particles precipitate within the grains. These extremely fine particles act as reinforcements, enhancing the mechanical properties of the sample. G. Nussbaum et al. [21] reported that the tensile properties of hot extruded samples could be significantly improved by the fine-grained alpha phase and the distribution of Mg17Al12 precipitations.
3. The grain size of FSW-processed samples is approximately twenty times smaller than that of the base metal grain size. According to the Hall-Petch relationship, which suggests an inverse relationship between hardness and grain size, the hardness and strength of FSW-processed samples increase [9, 10].

These factors collectively contribute to the mechanical properties of the FSW-processed samples. However, it's important to note that the interplay between these factors is complex and can vary depending on the specific process parameters used in FSW. For instance, the rate of cooling can influence the size and distribution of Mg17Al12 precipitations, which in turn can affect the mechanical properties of the samples. Similarly, the degree of plastic deformation during FSW can impact the final grain size, influencing the hardness and strength of the samples according to the Hall-Petch relationship.

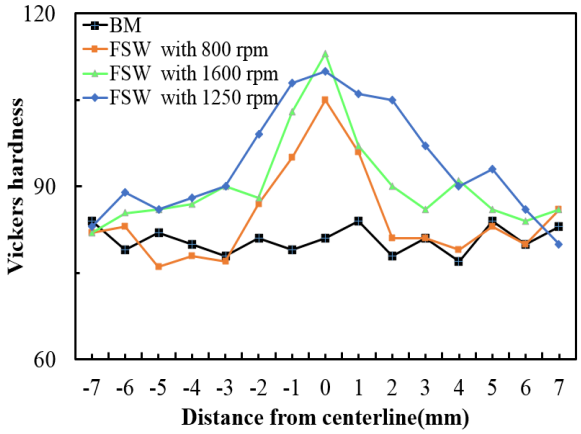

Fig. 10. Results of microhardness vs. distance from centerline, evaluation for the base metal and FSW-processed samples with different rotation speed and constant welding speed of 40 mm/min.

4. Conclusion

In this study, we investigated the influence of process parameters on the mechanical properties of AZ91C magnesium alloy joints produced by friction stir welding (FSW). The Taguchi L9 orthogonal array was employed to design the experimental matrix, and the input variables were systematically analyzed. Through the design of the experiments approach, we evaluated the ultimate tensile strength (UTS) and hardness (HV) for different combinations of tool rotation speed, welding speed, and plunge depth. The

main effects and interactions of the process parameters were analyzed to understand their individual and combined impacts on the mechanical attributes of the welded joints.

- The results of the experiments revealed a wide range of UTS and HV values, showcasing the significant influence of the diverse combinations of process parameters on the mechanical properties of the joints. Notably, we identified the optimal combination of process parameters for achieving the highest UTS and HV values, which were a tool rotation speed of 1250 rpm, welding speed of 40 mm/min, and a plunge depth of 0.3 mm.
- The interaction plots provided visual representations of the interactions between the process parameters, further highlighting the complex relationships between the factors in determining the mechanical properties of the FSW joints. Additionally, the signal-to-noise (S/N) ratio analysis was conducted, guiding us to the combinations of process parameters that lead to better mechanical performance.
- Microstructural evaluations of the base metal and stir zone (SZ) under various process conditions revealed the significance of FSW in refining the grain structure and improving the mechanical properties of the joints. The SZ exhibited a recrystallized equiaxed grain structure, resulting from the dynamic recrystallization (DRX) process occurring within the deformed region during FSW.
- The application of the Taguchi method enabled us to systematically analyze the effects of the process parameters on the mechanical properties of the AZ91C magnesium alloy joints. By considering the main effects and interactions of the input variables, which helped us optimize the FSW process parameters and identify the optimal conditions for achieving enhanced mechanical properties.
- In conclusion, this study highlights the importance of understanding and optimizing the FSW process parameters in order to enhance the mechanical properties of the AZ91C magnesium alloy joints. The application of the Taguchi method proved to be effective in systematically evaluating the effects of the process parameters and identifying the optimal conditions for improving the mechanical performance of the joints. The findings of this research provide valuable insights for further research and industrial applications of FSW in the automotive and aerospace industries.

Conflict of Interests

The authors declare that there is no conflict of interest.

Funding

The authors declare that no funds, grants, or other support were received during the preparation of this manuscript.

5. References

[1] B. Liu, J. Yang, X. Zhang, Q. Yang, J. Zhang, X. Li, Development and application of magnesium alloy parts for automotive OEMs: A review, Journal of Magnesium and Alloys, 11(1) (2023) 15-47.

[2] D. Kumar, L. Thakur, Influence of hybrid reinforcements on the mechanical properties and morphology of AZ91 magnesium alloy composites synthesized by ultrasonic-assisted stir casting, Materials today, 35 (2023), doi: 10.1016/j.mtcomm.2023.105937.

[3] A. Es'haghi Oskui, N. Soltani, Experimental and numerical investigation of the effect of temperature on mixed-mode fracture behaviour of AM60 Mg alloy, Fatigue and Fracture of Engineering Materials & Structures, (2019) 1-18.

[4] M.A. Unnikrishnan, J. Edwin Raja Dhas, K. Anton Savio Lewise, John C. Varghese, M. Ganesh, Challenges on friction stir welding of magnesium alloys in automotives, Materials Today: Proceedings, (2023), doi: 10.1016/j.matpr.2023.03.789.

[5] A.A. Luo, Magnesium casting technology for structural applications, Journal of Magnesium and Alloys, 1(1) (2013) 2-22.

[6] K. U. Kainer, Magnesium Alloys and their Applications, Deutsche Gesell schaft für Materialkunde, (2000).

[7] R.S Mishra, Z.Y. Ma, Friction stir welding and processing. Materials Science and Engineering: R: Reports, 50(1-2) (2005) 1-78.

[8] L. Liu, Welding and joining of magnesium alloys, Welding and Other Joining Technologies, (2010).

[9] P. Cavaliere, F. Panella, A. Squillace, Effect of welding parameters on mechanical and microstructural properties of AA6082 joints produced by friction stir welding, Journal of Materials Processing Technology, 180(1-3) (2006) 263-270.

[10] F. Chai, D.T. Zhang, Y.J. Li, Z.Q. Wu, Influence of welding parameters on microstructure and mechanical properties of friction stir welded Mg-Zn-Y-Zr alloy, Materials & Design, 46 (2013) 519-524.

[11] S. Rouhi, M. Shamanian, M. Esmailzadeh, Effects of welding environment on microstructure and mechanical properties of friction stir welded AZ91C magnesium alloy, Materials & Design, 35 (2012) 686-691.

[12] S. Malarvizhi, V. Balasubramanian, Influence of tool pin profile on microstructure and tensile properties of friction stir welded dissimilar aluminum alloys, Materials & Design, 32(6) (2011) 3613-3623.

[13] H. Sharankumar, V.J. Badheka, Effect of process parameters on tensile strength of friction stir welded aluminium matrix composite, Procedia Engineering, 97 (2015) 1837-1846.

[14] J. Singh, A. Chauhan, Optimization of friction stir welding parameters for dissimilar aluminum alloys using Taguchi technique, Procedia Engineering, 97 (2015) 2055-2062.

[15] D. Devaiah, K. Kishore, P. Laxminarayana, Optimal FSW process parameters for dissimilar aluminium alloys (AL 5083 and AL 6061) Using Taguchi Technique, Materials Today: Proceedings, 5 (2018) 4607–4614.

[16] R.S. Mishra, M.W. Mahoney, Friction Stir Welding and Processing, ASM International, (2007).

[17] K. Ranjit Roy, A Primer on the Taguchi Method, Society of Manufacturing Engineers (2010).

[18] P. Zolghadr, M. Akbari, P. Asadi, Formation of thermo-mechanically affected zone in friction stir welding, Materials Research Express, (2019), doi: 10.1088/2053-1591/ab1d25.

[19] M. Akbari, P. Asadi, Dissimilar friction stir lap welding of aluminum to brass: Modeling of material mixing using coupled Eulerian–Lagrangian method with experimental verifications, Proceedings of the Institution of Mechanical Engineers Part L Journal of Materials Design and Applications, 234(8) (2020) 1117-1128, doi:10.1177/1464420720922560.

[20] L. ížek, M. Gregera, L. Pawlicaa, L.A. Dobrzaskib, T. Taski, Study of selected properties of magnesium alloy AZ91 after heat treatment and forming, Journal of Materials Processing Technology 157-158 (2003) 466-471.

[21] G. Nussbaum, P. Bridot, T.J. Warner, J. Charbonnier, G. Regazzon, In magnesium alloys and their applications, B.L. Mordike and Hehmann, eds., DMG Informationsgesellshaft, Oberursel, (1992) 351-358.